TÜBİTAK

Turkish Journal of Chemistry

http://journals.tubitak.gov.tr/chem/

Research Article

Turk J Chem
(2018) 42: 1744 – 1754
© TÜBİTAK
doi:10.3906/kim-1712-42

Preparation of self-propelled Cu-Pt micromotors and their application in miRNA monitoring

Lütfi ÖKSÜZ[1], Gözde YURDABAK KARACA[2], Filiz KURALAY[3,*], Emre UYGUN[1], İsmihan Ümran KOÇ[1], Ayşegül UYGUN ÖKSÜZ

[1]Department of Physics, Faculty of Arts and Sciences, Süleyman Demirel University, Isparta, Turkey
[2]Department of Chemistry, Faculty of Arts and Sciences, Süleyman Demirel University, Isparta, Turkey
[3]Department of Chemistry, Faculty of Arts and Sciences, Ordu University, Ordu, Turkey

Received: 24.12.2017 • **Accepted/Published Online:** 06.06.2018 • **Final Version:** 06.12.2018

Abstract: Self-propelled catalytic micromotors offer considerable promise in terms of many applications. Catalytic micromotors are strongly influenced by the presence and concentration of specific ions and chemicals in the environment, making them useful as sensors and actuators. In this work, copper (Cu)-platinum (Pt) micromotors were fabricated by using the magnetron sputtering method for the first time in the literature and their applications based on the detection of miRNA-21 were evaluated. We analyzed the dependence of the mobility of Cu-Pt micromotors using different concentrations of hydrogen peroxide (H_2O_2). The presence of surfactants in the environment is also important for the movement of the micromotors. Thus, we studied the effect of three different surfactants: anionic as sodium dodecyl sulfate (SDS), cationic as cetyltrimethylammonium bromide (CTAB), and nonionic as Triton X-100. Cu-Pt micromotor motion was observed even at very low concentrations of surfactant (0.01%) and hydrogen peroxide (0.25%). miRNAs have been regarded as biomarker candidates in early diagnosis. Our sensing strategy relied on dye-labeled single-stranded DNA immobilization onto Cu-Pt micromotors that recognize the target miRNA-21. The changes in the fluorescence intensity as well as the changes in the speed of micromotors were examined before and after hybridization.

Key words: Micromotors, self-propelled micromotors, magnetron sputtering, miRNA-21

1. Introduction

Self-propelled catalytic micromotors receive considerable attention since they can convert energy into movement and force.[1,2] These devices have many different application fields such as drug delivery, environmental, biomedical, and sensing.[3,4] The shape, size, and material composition of the micromotors have a crucial influence on their application fields. An asymmetric micromotor structure containing a catalytic active part and an inert part is one of the common designs. For example, nanospheres with a half side coated with platinum (Pt) are propelled in hydrogen peroxide (H_2O_2) via a catalytic decomposition reaction.[5–8]

The fuel is very important for self-propelled catalytic micromotor applications.[9] H_2O_2 is the most commonly utilized fuel where the surface of the micromotors (i.e. platinum) catalyzes its decomposition to generate water (H_2O) and oxygen (O_2) bubbles. However, incompatible properties of H_2O_2 have hindered its operation *in vivo*.[10] Approaches to solve this problem include reducing the concentration of H_2O_2, using different biocompatible fuels, or using magnetic and ultrasound power for propelling.[11–13] As an example,

*Correspondence: kuralay.filiz@gmail.com

Sanchez et al. obtained micromotors working at low hydrogen peroxide concentrations (1% H_2O_2).[14] The work of Wang et al. demonstrated poly(3,4-ethylenedioxythiophene)/poly(3,4-ethylenedioxythiophene)-carboxylic acid/nickel/platinum (PEDOT/PEDOT-COOH/Ni/Pt) microjets that moved at 88 μm/s speeds and at 1% H_2O_2 fuel concentration.[15] It has been demonstrated that silica (SiO_2) particles worked at a speed of 35 μm/s in 5% H_2O_2 solution. Pumera et al. indicated that the average velocity of copper/silver (Cu/Ag) micromotors increased with the amount of H_2O_2 fuel present in the running solution from 13.1 μm/s in 0.5% H_2O_2 to 252.4 μm/s using 3% H_2O_2.[16]

The motion of chemically propelled micromotors depends on the rate at which bubbles are generated.[17,18] Surfactants also have a crucial role in the movement of bubble-propelled micromotors.[19] They can increase the interactions between the surface of platinum and H_2O_2 fuel with decreasing surface tension. Despite the efforts made regarding surfactant effect for microjects,[21] little attention has been given to the surfactant role for Janus micromotors relying on electrophoresis and diffusiophoresis.[19]

In this work, Cu-Pt bimetallic Janus micromotors were prepared in an alumina membrane by radiofrequency (RF) sputtering coating method. To the best of our knowledge, this is the first report describing the preparation of bimetallic Janus micromotors using RF sputtering, which allows the fast, homogeneous, and uniform distribution of metals. The effects of types and concentrations of surfactants on the speed of micromotors were investigated in the presence of anionic (sodium dodecyl sulfate, SDS), nonionic (Triton X-100), and cationic (cetyltrimethylammonium bromide, CTAB) surfactants. The prepared micromotors demonstrated long lifetime and excellent bubble propulsion motion, which can be detected even in the presence of a low concentration of hydrogen peroxide (0.25%). In a further step, miRNA sensing properties of bimetallic Janus Cu-Pt micromotors were examined based on fluorescence quenching and the decrease in micromotor speed with oligonucleotides related to breast cancer detection. In the literature, Ávilla et al. reported the use of graphene-oxide (GO)-coated gold nanowires (AuNWs) for intracellular miRNA detection.[21]

2. Results and discussion

2.1. Preparation and optimization studies of Cu-Pt bimetallic Janus micromotors

Cu-Pt bimetallic micromotors were prepared by coating Cu and Pt onto two sides of an alumina membrane using RF magnetron sputtering at 6.5 mTorr. Then their movements were captured with an optic microscope. Before that, we characterized the Cu-Pt micromotors in order to check their morphology and structure since they were synthesized with a new fabrication micromotor protocol. Catalytically propelled Cu-Pt bimetallic Janus micromotors were characterized by scanning electron microscopy (SEM) and energy dispersive X-ray spectroscopy (EDX) analysis. The bimetallic Janus micromotors have an average diameter of 30 μm (Figure 1a). As seen in Figure 1, the SEM and EDX mappings of the micromotor show the homogenous distribution of Cu (Figures 1b and 1c) and Pt (Figures 1b and 1d) components. Generally, Janus micromotors show a distribution of coated layers.[22] Guan et al. studied titanium dioxide/gold (TiO_2/Au) Janus micromotors and they found that the speed of the micromotor first increased when the size of the micromotor increased from 7.5 to 15 μm. Then the speed of the micromotor decreased as the size further increased to 22 and 30 μm.[23] Gao et al. fabricated Janus micromotors having diameters from 5 to 50 μm.[22] Wang et al. also demonstrated carbon/platinum Janus micromotors with an average diameter of 60 μm.[24] Micromotor diameter is dependent on the template or microspheres used and the coating methods.

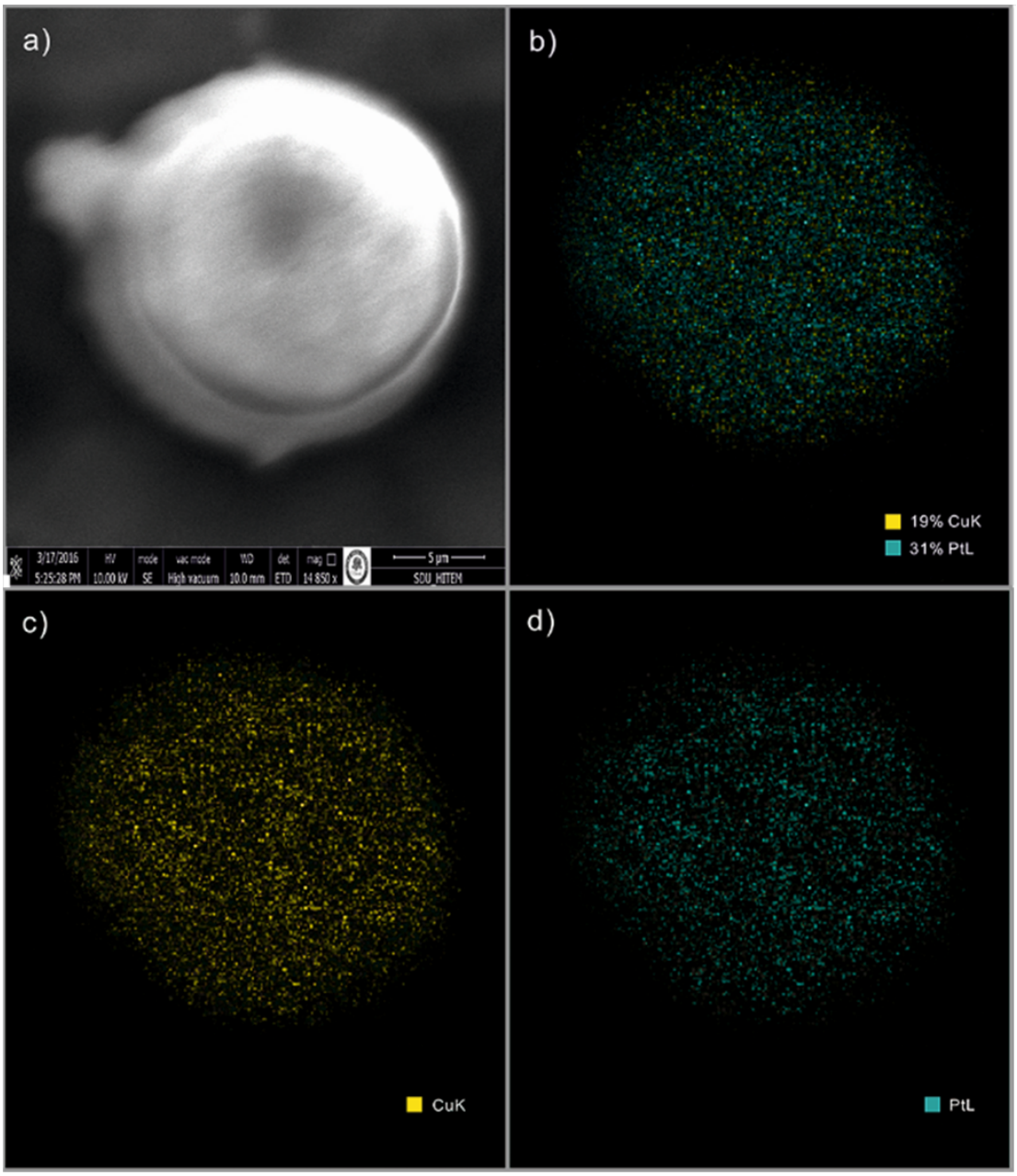

Figure 1. Characterization of Cu-Pt micromotor: SEM image of Cu-Pt micromotor (a), EDX mapping of Cu and Pt distribution (b), Cu distribution (c), Pt distribution (d).

In catalytic micromotors, fuel concentration has an important effect on the speed of the micromotor.[20,25] Low H_2O_2 concentrations have been desired especially for biomedical applications. Thus, we investigated the effect of H_2O_2 concentration and the influence of surfactant on the micromotor speed first. Figure 2 displays the speed of the Cu-Pt micromotors related to hydrogen peroxide (v/v) concentration. For comparison, the velocities of the micromotors were tracked with increasing concentration of hydrogen peroxide fuel (Figure 2a) in the presence of Triton X-100 surfactant. It is known that the speed of micromotors depends on the fuel concentration and generally increases with higher hydrogen peroxide concentrations.[21] Oxygen bubble

generation depends on the hydrogen peroxide concentration and the catalytic activity of the decomposition rate of peroxide into oxygen and water. The decomposition reaction (Eq. (1)) of hydrogen peroxide is shown below[26]:

$$2H_2O_2(aq) \xrightarrow{Pt} O_{2\,(g)} + 2H_2O \tag{1}$$

Micromotors started producing bubbles at a very low concentration of hydrogen peroxide (0.25%) and reached a high velocity of 120 μm/s (Figure 2a). The velocities of the Cu-Pt micromotors increased from 120 μm/s to 220 μm/s with elevated hydrogen peroxide fuel concentrations from 0.25% to 10%. Long lifetimes of 15 min were obtained at these high speed levels.[22]

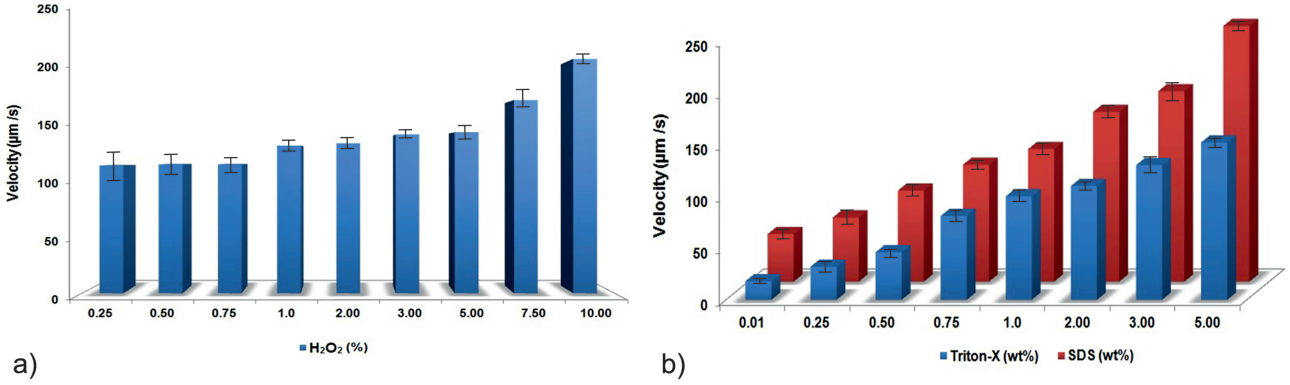

Figure 2. Speed of micromotors: hydrogen peroxide concentration vs. speed (a), surfactant concentration vs. speed of Cu-Pt micromotors (b) (n = 3).

Then the effect of surfactant on the movement of micromotors was examined with three different surfactants including SDS as anionic, Triton X-100 as nonionic, and CTAB as cationic. The Cu-Pt micromotors did not work in the presence of a wide range of concentrations (0.01% to 5%) of CTAB cationic surfactant. Both anionic and nonionic surfactants indicated positive effects on the speed of Cu-Pt micromotors. With increasing surfactant concentrations, the speed of micromotors increased significantly (Figure 2b). The performance of the surfactant in many interfacial processes depends on its concentration at the interface. Surfactant studies were carried out in an aqueous solution with a fixed concentration of hydrogen peroxide (0.25%). By comparing cationic, nonionic, and ionic surfactants, the anionic surfactant SDS indicated a much more positive effect on the speed of the micromotor. This could be related to the adsorption process of the surfactant molecules on the Pt surface. Anionic surfactant SDS can be easily adsorbed onto the positively charged inner surface of micromotors due to the attraction, while the cationic surfactant has to overcome repulsion to adsorb on the inner wall of micromotor. As a nonionic surfactant, Triton X-100 adsorbs from aqueous solution via moderate hydrophobic interaction with the uncharged platinum surface[19]. Therefore, the effectiveness of adsorption of cationic and nonionic surfactants onto positively charged inner surfaces of micromotors is lower than that of the anionic surfactant. At low concentrations (0.25%) of hydrogen peroxide, it is possible to generate enough oxygen bubbles for the propulsion of the Cu-Pt micromotors. Supplemental information (SI) Video 1 and SI Video 2 present the movement of Cu-Pt micromotors in the Triton X-100 and SDS surfactant media, respectively. As a bubble detaches from the surface, a new bubble is generated and released as long as the peroxide fuel is present in liquid medium.[25] The micromotor motion is influenced by the surrounding H_2O_2 and surfactant concentration.[27]

2.2. Application of Cu-Pt micromotors in miRNA monitoring

As far as we know, the fabrication of the Cu-Pt micromotors was performed with the simple magnetron sputtering method for the first time in the literature. These micromotors were then subjected to rapid, sensitive, and selective miRNA-21 detection related to breast cancer. The dye-labeled probe-immobilized micromotors recognized the target sequence in a very selective way. The experiments carried out with the 1-mismatch sequence (1-MM) showed that the micromotors were able to differentiate the target and 1-MM successfully. For the sensing methodology we aimed to track the speed of the micromotors and the fluorescence intensities before and after hybridization. The adsorption of fluorophore-labeled probe DNA interactions between the nucleotide bases and the nanomaterial led to quenching of the fluorescence.[21] FAM-labeled probe DNA exhibited strong fluorescence intensity after 60 min of incubation time at λ_{em} 520 nm, but movement of the micromotors was not observed (Figure 3). By measuring the speed and fluorescence intensities as dependent on incubation time, optimum incubation time was determined as 30 min for FAM-labeled probe DNA. The micromotor movement speed was 112 μm/s and fluorescence intensity was 431.

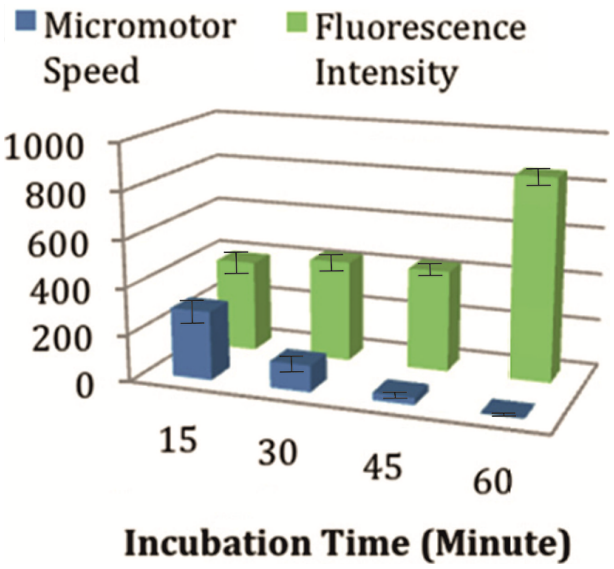

Figure 3. Cu-Pt micromotor interaction with FAM-labeled probe DNA. Green bars and blue bars represent fluorescence intensity and speed of micromotors with respect to increasing incubation time, respectively (n = 3).

Related microscopic images for Cu-Pt micromotors and FAM-labeled probe DNA immobilized Cu-Pt micromotors (FAM-ssDNA/Cu-Pt) are given in Figure 4a and b, respectively.

After the optimization of FAM-labeled probe DNA incubation time, we examined the changes in the micromotor speed and the fluorescence intensity. Various conditions were optimized to achieve the best miRNA responsive performance. To show the applicability of the micromotor approach toward miRNA detection, we compared the fluorescence signals observed after incubating the FAM-ssDNA on Cu-Pt micromotors with different molar concentrations of the synthetic target miRNA-21 for 30 min of hybridization time. As illustrated in Figure 5a (a green bar), the fluorescence signal is higher in the absence of the target miRNA-21 than in the presence of the target miRNA-21 (Figures 5b and 5c). Increasing along with the target concentration from 5 nM to 100 nM, the micromotor speed decreased from 277 μm/s to 140 μm/s, respectively (Figure 5d). The detection limit was calculated as 0.56 nM, which suggested the use of these micromotors for early cancer diagnosis (based

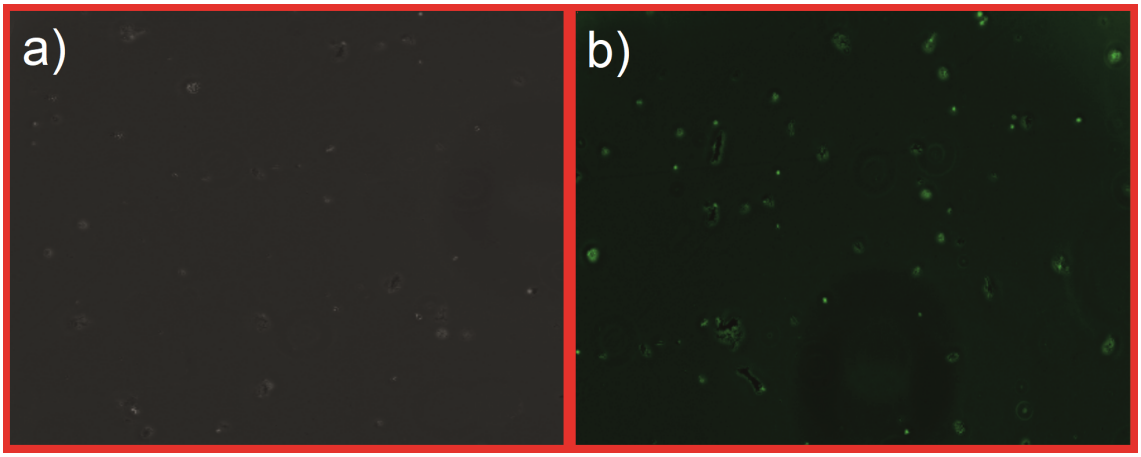

Figure 4. Microscope images (40 × optics) of (a) Cu-Pt and (b) FAM-labeled probe DNA/Cu-Pt micromotors.

on the changes in the speed).[28] The calibration graph of the study is given in Figure 5e. The reproducibility was examined using 5 nM target miRNA-21. The RSD was found as 5.4% (n = 3), giving a promising result for clinical applications. Both fluorescence signals and the speed of the micromotors decreased after incubating the target miRNA-21 (100 nM) for different incubation times. These results demonstrate that the quenching of the fluorophore can occur due to the close proximity of the target sequence due to an internal hybrid formation with the probe.[29] This reflects the quenching efficiency of Cu-Pt micromotors and hybridization efficiency of the target miRNA-21 with the FAM-ssDNA probe immobilized on the Cu-Pt micromotors. Related microscopic images are given in Figures 6a–6d, as well.

Related videos according to the 100 nM target for 5, 15, and 30 min of incubation time are given as SI Video 3. The Table shows the comparison of the studies related to miRNA detection based on various nanomaterials.[21,30–32]

Table. Comparison of the work with the literature.

Nano/micromaterials	Detection limit	Reference
GO coated AuNWs nanomotors	Not calculated (experiments were carried out with 100 nM miRNA-21)	22
Molybdenum disulfide (MoS_2) nanosheets	Not calculated (experiments were carried out with 10 nM miRNA)	31
GO	9 pM	32
Gold nanoparticles-coated magnetic beads (AuNPs-MBs)	9 fM	33
Cu-Pt micromotors	0.56 nM	This study

Furthermore, the selectivity of the Cu-Pt micromotor for miRNA-21 detection was evaluated by comparing the fluorescence signal for the miRNA-21 target and the signal obtained for the 1-MM sequence. The Janus micromotors easily differentiated the miRNA-21 target and 1-MM (Figure 7). This result indicates that the Cu-Pt micromotor is quite selective for the miRNA-21 target sequence. Our findings demonstrated that the micromotor detection strategy has the potential to observe the dynamic changes of miRNA detection with FAM-ssDNA functionalized Cu-Pt micromotors for real-time future clinical applications such as early and rapid cancer diagnosis.[33]

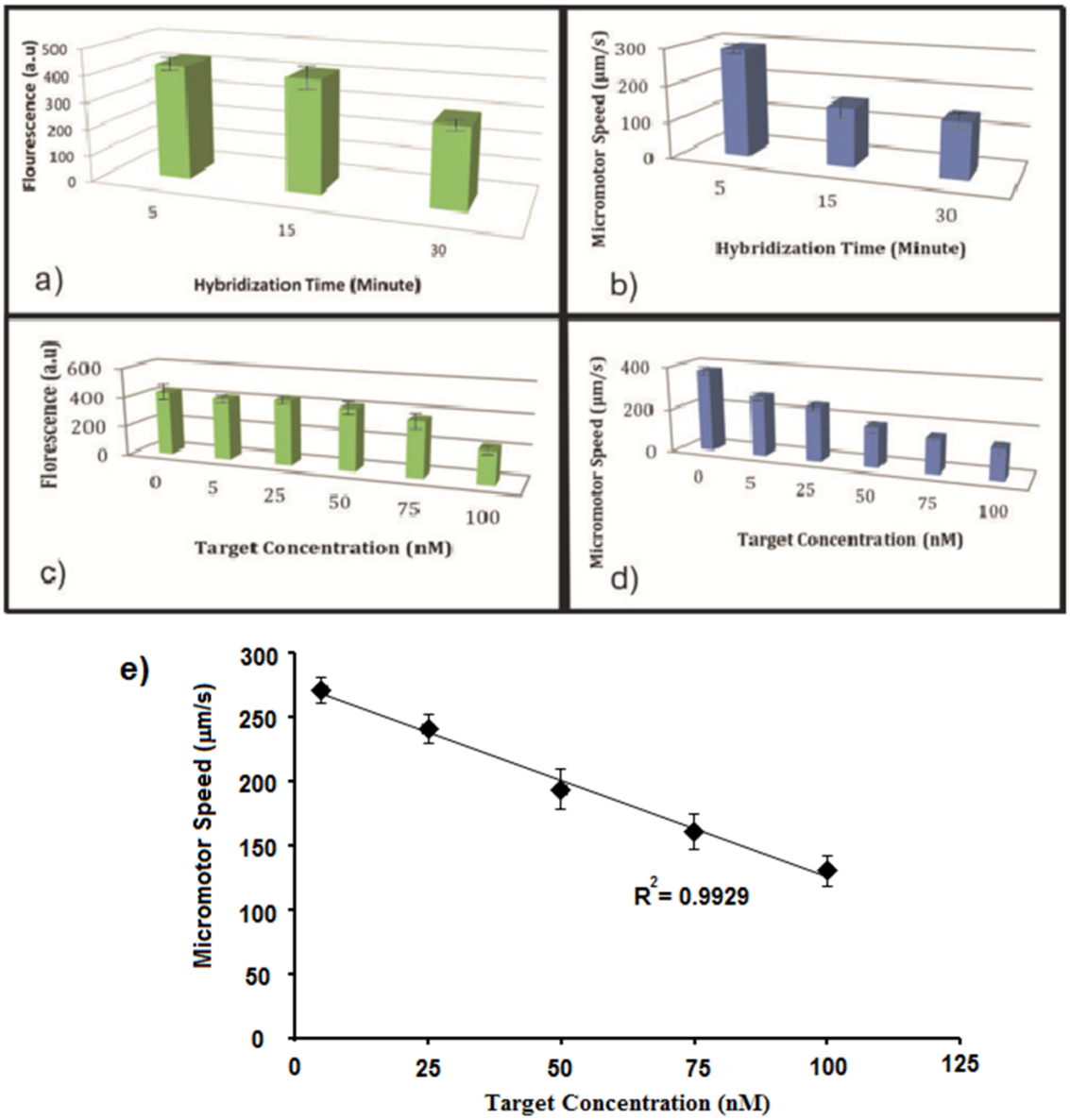

Figure 5. Target hybridization time effect at 100 nM on fluorescence intensity (a) and on micromotor speed (b); target concentration effect on fluorescence intensity (c) and on micromotor speed (d) at 30 min of hybridization time; (e) calibration graph (n = 3).

2.3. Conclusions

In the first part of the study, movement properties of Cu-Pt bimetallic micromotors were investigated depending on concentrations of the hydrogen peroxide fuel and surfactant media. The speed of Cu-Pt bimetallic micromotors was affected strongly by the addition of surface tension-reducing agents such as SDS and Triton X-100 to enhance bubble formation in order to analyze the concentration effect. The prepared Cu-Pt micromotor was moved at low concentrations (0.25%) of the hydrogen peroxide and demonstrated excellent bubble-propelled motion. In the second step of the study, we presented a micromotor-based strategy for rapid monitoring of miRNA-21 detection. Cu-Pt micromotor fluorescence intensity and speed changed due to the absence and

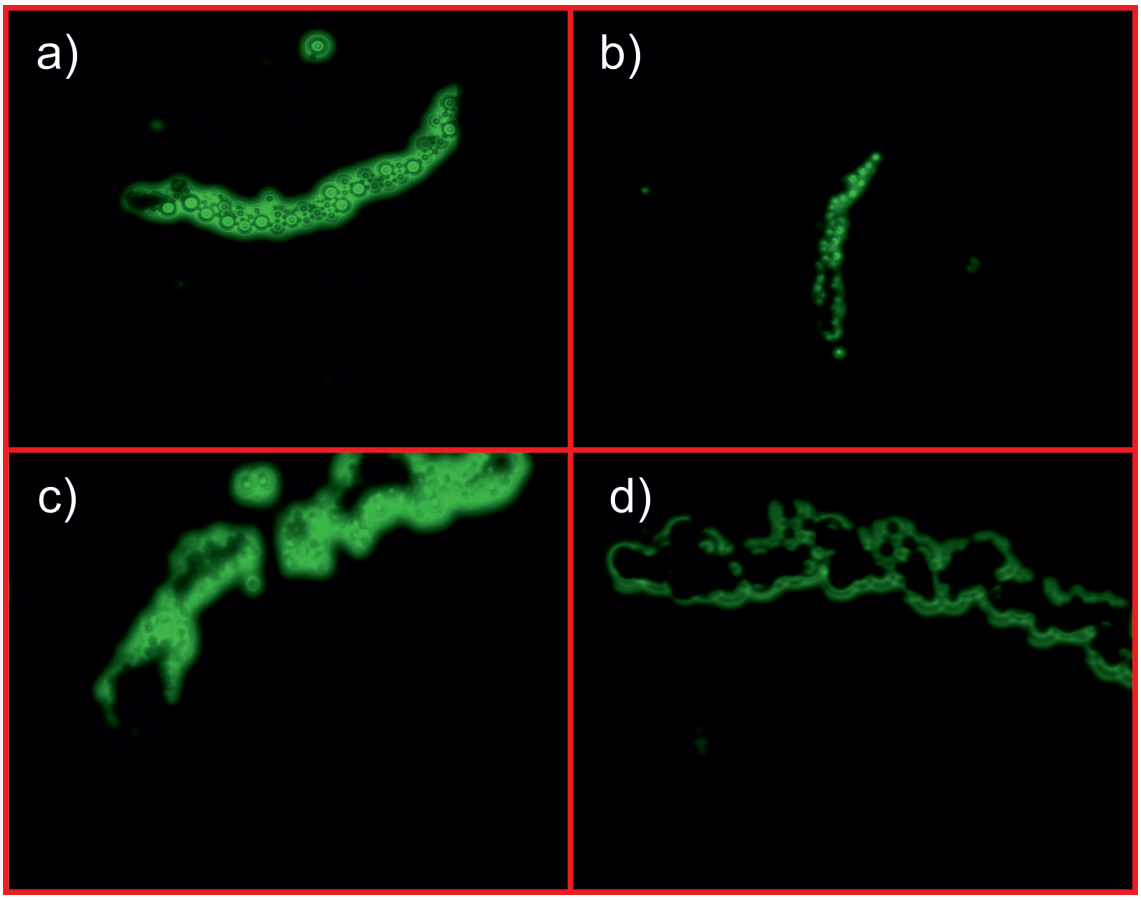

Figure 6. Microscope images of (a) FAM-labeled ssDNA/Cu-Pt, (b) FAM-labeled ssDNA/Cu-Pt for 5 min of target hybridization, (c) 15 min of target hybridization, (d) 30 min of target hybridization (target concentration: 100 nM).

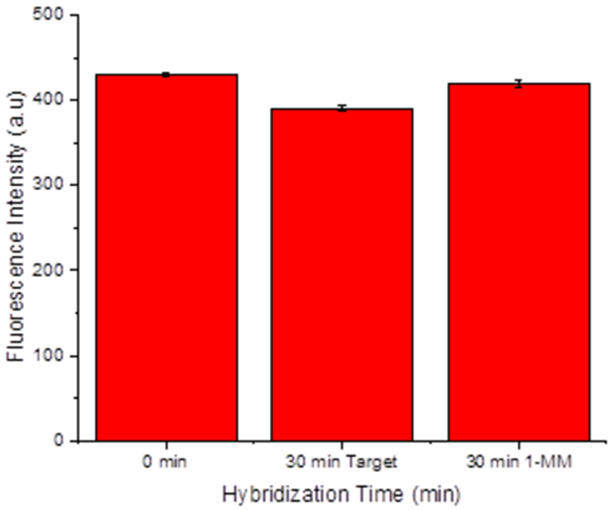

Figure 7. Results for selectivity (n = 3).

presence of the target miRNA-21. The most important advantage of using this novel Cu-Pt micromotor for miRNA-21 sensing may be its rapid detection (even in 5 min) and selective recognition of the target. In addition,

the high speed ability of FAM-ssDNA functionalized Cu-Pt micromotors can make it possible to detect target cancer cells for real-time applications. These micromotors are very promising in early cancer diagnostics.

3. Experimental

3.1. Materials

The alumina membranes with pores of 25 mm in diameter (pore size: 0.2 μm) were purchased from Whatman (6809-6022). Cu and Pt targets from China Leadmat Advanced Materials Co. Ltd. (diameter: 5.08 cm; thickness: 0.635 cm) were used for the magnetron sputtering process. Hydrogen peroxide (30%) and sodium hydroxide were purchased from Sigma-Aldrich. SDS, CTAB, and Triton X-100 were purchased from Fluka. Oligonucleotides were supplied from Heliks Biotechnology (Turkey):

FAM-ssDNA antimiRNA-21 Probe: FAM-5'-TCAACATCAGTCTGATAAGCTA-3'
Target miRNA-21: 5'-UAGCUUAUCAGACUGAUGUUGA-3'
1-Base mismatch sequence (1-MM): 5'-UAGCUUAUAAGACUGAUGUUGA-3'

3.2. Fabrication of micromotors

One side of the Al membrane was coated with Cu and the other side was coated with Pt by the RF magnetron sputtering method. Sputtering base pressure was 2 mTorr and working pressure was 6.5 mTorr. Sputtering parameters were 25 W and 1 h for both sides under argon gas flow. The distance between target and substrate was kept constant at 9.5 cm for all sputtering processes. The sputtered Cu layer was completely removed by hand polishing with alumina slurry of 3–4 μm. The membrane was dissolved in 3 M sodium hydroxide (NaOH) solution for 30 min in order to remove the membrane. The latter was collected by centrifugation at 6000 rpm for 20 min. This procedure was repeated three times, and then pure water cleaning was started at 6000 rpm for 5 min three times. Figure 8 presents the preparation steps of the Janus micromotors. Characteristic properties of the micromotors were investigated with a Nikon Eclipse Ti Optic LV100ND Model microscope.

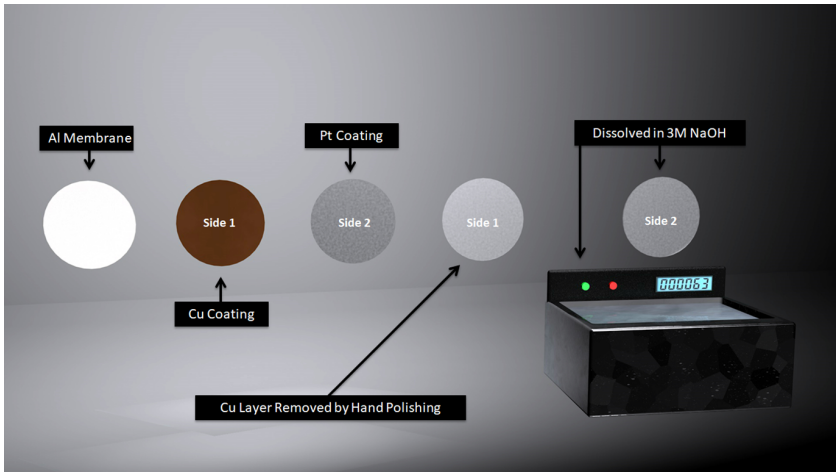

Figure 8. Preparation protocol of Janus Cu-Pt structure.

3.3. 6-Carboxyfluorescein (6-FAM) dye-labeled probe DNA immobilization

Micromotors were centrifuged at 6000 rpm for 5 min and pure water was taken carefully. Then 10 μL of dye-labeled probe DNA (53.3 μM) was incubated with micromotors and held for 30 min. After the incubation process, 50 μL of 20 mM Tris-HCl, pH 7.4, containing 100 mM NaCl, 1 mM EDTA, and 100 μg/mL of BSA, was used to perform the washing steps.

3.4. miRNA detection

The miRNA-21 detection protocol involved the duplex formation (hybridization). To perform these experiments, 10 μL of 100 nM of the synthetic target miRNA-21 (prepared in 20 mM Tris-HCl buffer, pH 7.4, containing 100 mM NaCl, 5 mM KCl, and 5 mM $MgCl_2$) was added to the FAM-ssDNA probe immobilized Cu-Pt micromotors and different incubation times (5, 15, 30, and 60 min) were studied.

The effect of target concentration (5, 25, 50, 75, and 100 nM) was investigated at a constant incubation time of 30 min. After that, the sample fluorescence signals were measured with a microscope (Nikon Eclipse Optic LV100ND microscope). A selectivity experiment was carried out with a 1-MM sequence having a concentration of 500 nM at 30 min of hybridization time. Figure 9 shows the miRNA detection steps of the Janus Cu-Pt micromotors.

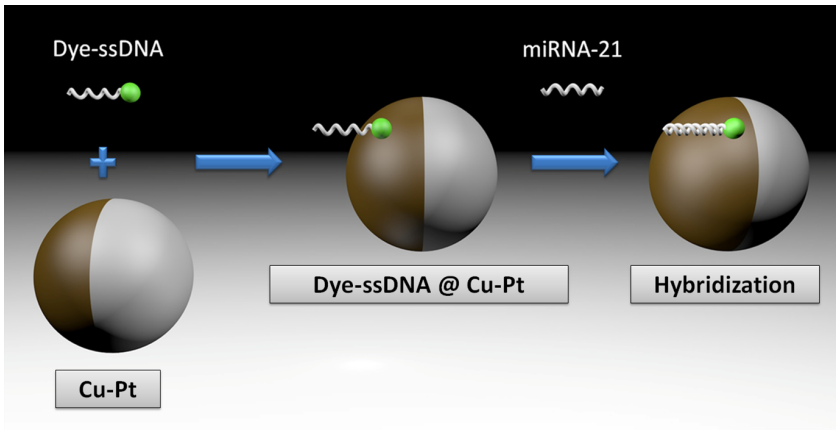

Figure 9. miRNA detection protocol with Cu-Pt Janus micromotors.

Videos and images were captured using an Andor Zyla VSC-02912 camera with 40 × and 60 × objectives. A Nikon Eclipse Ti upright microscope with DPI filter (S Plan Fluor ELWD 40 × Ph2 ADM, S Plan Fluor ELWD 60 × Ph2 ADL) was used to capture fluorescence images.

Acknowledgments

The authors gratefully acknowledge TÜBİTAK (Project No: 1150098) and Plazmatek for financial support of this study. F.K. acknowledges Turkish Academy of Sciences (TÜBA) as an associate member and TÜBA-GEBİP Program.

References

1. Singh, V.V.; Wang, J. *Nanoscale* **2015**, *7*, 19377-19389.
2. Li, L.; Wang, J.; Li, T.; Song, W.; Zhang, G. *Soft Matter* **2014**, *10*, 7511-7518.

3. Wang, E. C.; Wang, A. Z. *Integr. Biol.* **2014**, *6*, 9-26.
4. Guix, M.; Meyer, A. K.; Koch, B.; Schmidt, O. G. *Sci. Rep.-UK* **2016**, *6*, 21701.
5. Ma, X.; Hahn, K.; Sanchez, S. *J. Am. Chem. Soc.* **2015**, *137*, 4976-4979.
6. Ke, H.; Ye, S.; Carroll, R. L.; Showalter, K. *J. Phys. Chem. A* **2010**, *114*, 5462-5467.
7. Gibbs, J.; Zhao, Y. *Front. Mater. Sci.* **2011**, *5*, 25-39.
8. Dong, R.; Li, J.; Rozen, I.; Ezhilan, B.; Xu, T.; Christianson, C.; Gao, W.; Saintillan, D.; Ren, B.; Wang, J. *Sci. Rep.-UK* **2015**, *5*, 13226.
9. Men, Y.; Peng, F.; Wilson, D. A. *Science Letters Journal* **2016**, *5*, 219.
10. Li, J.; Rozen, I.; Wang, J. *ACS Nano* **2016**, *10*, 5619-5634.
11. Katuri, J.; Ma, X.; Stanton, M. M.; Sánchez, S. *Accounts Chem. Res.* **2017**, *50*, 2-11.
12. Magdanz, V.; Guix, M.; Schmidt, O. G. *Robotics and Biomimetics* **2014**, *1*, 11.
13. Jurado-Sánchez, B.; Escarpa, A. *TrAC-Trend. Anal. Chem.* **2016**, *84*, 48-59.
14. Sanchez, S.; Ananth, A. N.; Fomin, V. M.; Viehrig, M.; Schmidt, O. G. *J. Am. Chem. Soc.* **2011**, *133*, 14860-14863.
15. García, M.; Orozco, J.; Guix, M.; Gao, W.; Sattayasamitsathit, S.; Escarpa, A.; Merkoçi, A.; Wang, J. *Nanoscale* **2013**, *5*, 1325-1331.
16. Teo, W. Z.; Wang, H.; Pumera, M. *Chem. Commun.* **2016**, *52*, 4333-4336.
17. Zhao, G.; Sanchez, S.; Schmidt, O. G.; Pumera, M. *Nanoscale* **2013**, *5*, 2909.
18. Gibbs, J. G.; Zhao, Y. P. *Appl. Phys. Lett.* **2009**, *94*, 163104.
19. Wang, H.; Zhao, G.; Pumera, M. *J. Phys. Chem. C* **2014**, *118*, 5268-5274.
20. Simmchen, J.; Magdanz, V;. Sanchez, S.; Chokmaviroj, S.; Ruiz-Molina, D.; Baeza, A.; Schmidt, O. G. *RSC Adv.* **2014**, *4*, 20334-20340.
21. Ávila, B. E. F. C. A. D.; Martín, A.; Soto, F.; Lopez-Ramirez, M. A.; Campuzano, S.; Vásquez-Machado, G. M.; Gao, W.; Zhang, L.; Wang, J. *ACS Nano* **2015**, *9*, 6756-6764.
22. Gao, W.; D'Agostino, M.; Garcia-Gradilla, V.; Orozco, Wang, J. *Small* **2013**, *9*, 467-471.
23. Li, Y.; Mou, F.; Chen, C.; You, M.; Yin, Y.; Xu, L.; Guan, J. *RSC Adv.* **2016**, *6*, 10697-10703.
24. Jurado-Sánchez, B.; Sattayasamitsathit, S.; Gao, W.; Santos, L.; Fedorak, Y.; Singh, V. V.; Orozco, J.; Galarnyk, M.; Wang, J. *Small* **2015**, *11*, 4, 499-506.
25. Wang, J. *Nanomachines: Fundamentals and Applications*; Wiley-VCH: Weinheim, Germany, 2013.
26. Valadares, L. F.; Tao, Y.; Zacharia, N. S.; Kitaev, V.; Galembeck, F.; Kapral, R.; Ozin, G. A. *Small* **2010,** *6*, 565-572.
27. Banerjee, S. S.; Jalota-Badhwar, A.; Zope, K. R.; Todkar, K. J.; Mascarenhas, R. R.; Chate, G. P.; Khutale, G. V.; Bharde, A.; Calderon, M.; Khandare, J. J. *Nanoscale* **2015**, *7*, 8684-8688.
28. McCreery, R. L. In *Electroanalytical Chemistry*; Bard, A. J., Ed. Marcel Dekker: New York, NY, USA, 2007, pp. 221-374.
29. Marras, S. A. E. In *Fluorescent Energy Transfer Nucleic Acid Probes*; Didenko, V., Ed. Humana Press: New York, NY, USA, 2006, pp. 3-16.
30. Oudeng, G.; Au, M.; Shi, J.; Wen, C.; Yang, M. *ACS Appl. Mater. Inter.* **2018,** *10*, 350-360.
31. Cui, L.; Lin, X.; Lin, N.; Song, Y.; Zhu, Z.; Chen, X.; Yang, C. *Chem. Commun.* **2012**, *48*, 194-196.
32. Wei, T.; Du, D.; Wang, Z.; Zhang, W.; Lin, Y. *Biosens. Bioelectron.* **2017,** *94*, 56-62.
33. de Ávila, B.E. F.; Angell, C.; Soto, F.; Lopez-Ramirez, M. A.; Báez, D. F.; Xie, S.; Wang, J.; Chen, Y. *ACS Nano* **2016**, *10*, 4997-5005.

Supplemental information

SI Video 1. Cu-Pt micromotor movement in the presence of nonionic surfactant Triton-X 100 (0.01%) with H_2O_2 (0.25%) fuel: http://

SI Video 2. Cu-Pt micromotor movement in the presence of anionic surfactant SDS (0.01%) with H_2O_2 (0.25%) fuel: http://

SI Video 3. FAM-ssDNA/Cu-Pt micromotors speed and fluorescence intensity after 5, 15, and 30 min of target (100 nM) hybridization and before target incubation: http://